RMetS
Royal Meteorological Society

On the connection between tropical circulation, convective mixing, and climate sensitivity

L. Tomassini,[a]* A. Voigt[b]† and B. Stevens[a]
[a]*Max Planck Institute for Meteorology, Hamburg, Germany*
[b]*Laboratoire de Météorologie Dynamique, Université Pierre et Marie Curie, Paris, France*

*Correspondence to: L. Tomassini, Max Planck Institute for Meteorology, Bundesstrasse 53, D-20146 Hamburg, Germany.
E-mail: lorenzo.tomassini@mpimet.mpg.de

The connection between the large-scale tropical circulation of the atmosphere, convective mixing, and climate sensitivity is explored in a wide range of climates through a perturbed-parameter ensemble of a comprehensive Earth System Model. Four parameters related to the representation of atmospheric moist convection are found to dominate the response of the model. Their values govern the strength of the tropical circulation, the surface temperature, atmospheric humidity, and the strength of the tropical overturning circulation, largely through their influence on the atmospheric stability. The same convective parameters, albeit in different combinations, also have a strong influence on the equilibrium climate sensitivity of the model, which ranges from a little over 3 °C to more than 10 °C. The importance of the most poorly represented processes in determining important aspects of the behaviour of the model argues for the need to move beyond statistical approaches to estimating climate sensitivity and to focus on the development of a better understanding and representation of convective mixing, particularly in the Tropics.

Key Words: tropical circulation; convection parametrization; convective mixing; climate sensitivity

Received 19 February 2014; Revised 19 June 2014; Accepted 1 September 2014; Published online in Wiley Online Library

1. Introduction

Diagnostic studies have long shown that shallow marine boundary-layer (MBL) clouds play an important role in setting the climate sensitivity of comprehensive models of climate change, particularly in the Tropics where their effect on short-wave radiation is strongest (Bony and Dufresne, 2005; Webb *et al.*, 2006; Medeiros *et al.*, 2008; Vial *et al.*, 2013). Models which develop a large temperature response to rising concentrations of atmospheric CO_2 tend to be characterized by a strong reduction in marine boundary-layer clouds, while models that warm more modestly are usually associated with a smaller decrease, or even an increase, in the amount of MBL cloud. No other factor appears to be as important for explaining the spread in estimates of the equilibrium climate sensitivity of comprehensive climate models.

However a number of recent studies have questioned the inference that it is the physics of the representation of these clouds which determine climate sensitivity by showing that changes in climate sensitivity are closely tied to changes in the large-scale circulation (e.g. Fasullo and Trenberth, 2012; Stevens and Bony, 2013b; Sherwood *et al.*, 2014). Although changes in the overturning tropical circulation, as measured by the strength of the Hadley and Walker cells and the extent of the Hadley cell, are expected to accompany changes in the globally averaged surface temperatures, the recent work suggests that the structure of the large-scale circulation plays a more primary role in determining the response of the climate system to perturbations.

For instance, Fasullo and Trenberth (2012) show that the strength of the tropical circulation, which they measure by seasonal variations in the lower-troposphere relative humidity, is strongly linked to projected cloud trends, and hence climate sensitivity in models. Sherwood *et al.* (2014) further suggest that mixing processes in regions of deep convection are important in determining the response of models to warming. Perturbed physics experiments also consistently identify convective entrainment parameters related to deep convection, which is closely tied to the structure of the large-scale circulation (e.g. Möbis and Stevens, 2012), as the most important parameters for the sensitivity of individual climate models (Collins *et al.*, 2010; Joshi *et al.*, 2010; Zhao, 2014).

The idea that the representation of deep convection, which is so intimately connected to the structure of the tropical circulation itself, might be important for the response of the climate system to warming is not surprising. To a first approximation, the tropical atmosphere can be viewed as being governed by deep convection responding to the destabilization of the atmosphere by radiative cooling from water vapour (Emanuel *et al.*, 1994; Stevens and Bony, 2013a), with models that capture this basic balance being able to reproduce, to a surprising extent, the structure of the tropical atmosphere even when a great many more additional, and complicating, processes are neglected (Popke *et al.*, 2013).

†Current address: Lamont-Doherty Earth Observatory, Columbia University, New York, USA.

Nonetheless, deep convection is often assumed to be along for the ride. Large-scale dynamical studies often attempt to understand the response of the circulation to external forcing, such as meridional gradients in solar insolation or sea-surface temperatures, given a particular ansatz for deep convection (Held and Hou, 1980; Schneider and Walker, 2008). In such studies the assumption is that the particular representation of deep convection is not crucial to the response of the system to changes in forcing. Likewise, thermodynamic studies that adopt the viewpoint of the cloud radiative effect note that, due to a large cancellation between the short-wave and long-wave components, the net radiative effect of deep convective clouds is nearly zero (Hartmann and Short, 1980). As a result, these studies tend to focus on cloud regimes which project more strongly on to the top of the atmosphere (TOA) radiative balance, and thus on the role of shallow convection.

In this study, influenced by the recent literature suggesting a stronger link between the structure of the large-scale tropical circulation, the climate and the climate response to forcing, we step back from a more narrow focus on shallow convection to explore how the representation of convective mixing processes more broadly influences these links. In doing so, we turn the tables not only on the traditional approach to studying climate sensitivity, with its strong emphasis on processes regulating the behaviour of shallow convection, but also on studies in large-scale tropical dynamics, which take the representation of convective mixing processes for granted. Our premise is that to understand the variety of climate sensitivity estimates from models, it is necessary to understand the connection between parametrized convective mixing and the large-scale tropical circulation. To do so, we systematically investigate these relationships in a coupled climate model, the Max Planck Institute Earth System Model (MPI-ESM), by varying a few key properties of the convection parametrization. This allows the sharpening of our understanding of the interplay between convective mixing and the large-scale tropical circulation, and examines possible implications for model climate sensitivity.

The purpose of using a perturbed parameter approach is that it allows the close control of the changes in the physical process representation that are applied to the model, and thus investigates the implications of these confined modifications for climate and climate sensitivity. The aim of the study is thus not to broadly sample structural model uncertainty as present in a multi-model ensemble. Instead, we focus on key physical connections between important parametrized subgrid-scale convective processes, the control state, and climate sensitivity in a coupled general circulation model (GCM).

In section 2 we introduce the coupled climate model and the experimental design, and give a description of the parameters which are varied to generate an ensemble of model configurations. We also describe the primary radiative effects of the varied parameters. In section 3 we explore how the moisture and cloud cover characteristics in pre-industrial climates relate to features of the large-scale tropical circulation. In section 4 the effect of the most important parameters on the main characteristics of the pre-industrial climates is examined in more detail. Section 5 deals with the question how the properties of the pre-industrial climates relate to climate sensitivity. Our conclusions are summarized in section 6.

2. Climate model and experiments

2.1. Climate model simulations

The simulations are performed with a coarse-resolution version of the MPI-ESM (Giorgetta *et al.*, 2013). This version of the model is usually reserved for instructional purposes, but is used here for reasons of computational efficiency. The version of the MPI-ESM employed in the present study consists of the atmosphere GCM ECHAM6.0.4 (Stevens *et al.*, 2013), here used in the coarse resolution T31/L19-version, and the ocean GCM MPI-OM (Jungclaus *et al.*, 2013) in GR30/L40 resolution. Two structural changes from the ECHAM6* version described in Stevens *et al.* (2013) include a minor technical bug fix in the atmospheric convection scheme and the use of an extension of the orographic gravity wave drag parametrization which includes mountain lift forces (Lott, 1999). The latter is not necessary in higher-resolution versions of ECHAM6 but improves the atmospheric circulation of the Northern Hemisphere midlatitudes when the model is run in coarse resolution. ECHAM6 employs a slightly modified version of the Tiedke–Nordeng convection scheme (Tiedtke, 1989; Nordeng, 1994) which is thoroughly described in Möbis and Stevens (2012).

MPI-ESM, hereafter the model, is integrated for 3000 years under pre-industrial conditions in a configuration that applies the model's standard parameters. This configuration will be called 'standard configuration' in the remainder of the article. At the end of the spin-up, the climate is essentially stationary with small trends limited to the deep ocean. These trends are irrelevant to the questions addressed here.

Starting from the end of the spin-up simulation, a 600-year long pre-industrial 'standard' simulation with the standard configuration of the model is performed. One hundred additional model configurations are generated by varying the values of key atmospheric parameters related to atmospheric mixing and several oceanic parameters. For each of these model configurations, a 600-year long pre-industrial simulation is performed as well, yielding a total of 101 model configurations and pre-industrial simulations. For the analysis, the last 50 years are used. From these 101 configurations, only those that simulate global mean near-surface temperatures between 8 and 17 °C are analyzed further; this restriction is made to minimize differences in sea ice and hence surface albedo. Sixty-six out of 101 model configurations meet this criterion, and these simulations constitute what we hereafter refer to as the perturbed parameter ensemble. The restriction to the mentioned temperature range does not imply that the ensemble considered in the present study is a good analogue for a multi-model ensemble of pre-industrial control simulations with structurally different, tuned global climate models. Rather, the aim of this restriction is to exclude extreme climates in which processes that are marginal under moderate conditions might become important.

To diagnose the climate sensitivity of the 66 model configurations, idealized 'abrupt $4\times CO_2$' climate change simulations are performed according to the CMIP5† 'abrupt $4\times CO_2$' experiment (Taylor *et al.*, 2012). These simulations are started from their respective pre-industrial simulations and are integrated for 150 years.

2.2. Description of varied parameters and their radiative effects

The different model configurations are obtained by varying eight important but poorly constrained parameters of MPI-ESM, some of which are used to tune the model (Mauritsen *et al.*, 2012). The global-mean climate of the atmosphere and the surface turns out to be mostly determined by four of these parameters, and the present study will focus on these. All these four parameters belong to the atmospheric convection parametrization and are described in Tiedtke (1989). The remaining four parameters affect orographic wave drag and ocean mixing; they are briefly introduced below, but will not be considered in the rest of the article. Instead, we view them to generate a background variability against which the robustness of the impacts of the convective parameters can be assessed. Table 1 gives an overview of all eight parameters, their values as used in the standard model configuration, and the range over which they are varied.

*ECHAM: ECMWF model, Hamburg version.
†CMIP: Coupled Model Intercomparison Project.

Table 1. Parameters varied to generate the different model configurations, and the model component to which they are applied.

Parameter	Default	Range		Component	Code name
CloudOvershoot	0.23	0.11 to 0.35		Convection (Atm)	cmfctop
EntrainShallow	3×10^{-4}	3×10^{-5}	3×10^{-3}	Convection (Atm)	entrscv
EntrainDeep	1×10^{-4}	1×10^{-5}	1×10^{-3}	Convection (Atm)	entrpen
AutoConversion	8×10^{-4}	8×10^{-5}	8×10^{-3}	Convection (Atm)	cprcon
OroLift	1.0	0	1.0	Gravity Waves (Atm)	gklift
OceanMixBack	1.05×10^{-5}	1.05×10^{-6}	1.05×10^{-4}	Mixing (Ocn)	dback
OceanMixRich	0.002	0.0001	0.04	Mixing (Ocn)	dv0
OceanMixEddy	500	100	2500	Mixing (Ocn)	ibolk

Atm = atmosphere; Ocn = ocean.

The parameters *CloudOvershoot*, *OroLift*, and *OceanMixEddy* are sampled according to a uniform distribution, the other parameters are assumed to be distributed log-normally. A low-discrepancy quasi-random number algorithm is used for the generation of the eight-dimensional sample (Bratley and Fox, 1988). Only sample points for which *EntrainDeep* is smaller than *EntrainShallow* are accepted.

In the following we briefly describe the parameters' physical meanings. For the atmospheric convection parameters, which are the focus of the present study, we will also discuss their impacts on the TOA radiation budget (also Mauritsen *et al.*, 2012).

With respect to the radiation balance, the main effect of shallow convection is to export cloud water from the boundary layer to regions immediately above. The resulting evaporative cooling just above the boundary layer acts to reduce the stratification and promotes the mixing and deepening of the layer (Betts, 1973; Stevens, 2007). The strength of this effect is influenced mainly by two convective parameters. The convective mass flux above the level of neutral buoyancy, *CloudOvershoot*, determines the fraction of convective mass flux that is detrained in the model level above the level of neutral buoyancy. The parameter is not only used for deep but also for shallow convection; thus increasing it reduces and thins boundary-layer cloud and increases the amount of absorbed short-wave irradiance. The other parameter, the entrainment rate for shallow convection, *EntrainShallow*, has the opposite effect on cloud and the radiation balance. Increasing *EntrainShallow* dilutes and weakens updraughts; as a result less cloud liquid water is exported out of the boundary layer and boundary-layer clouds increase in areal coverage and thickness. *EntrainShallow* may act on convective clouds which are in fact quite deep because of the way the convection scheme separates shallow from deep convective processes (Möbis and Stevens, 2012).

The lateral entrainment rate for deep convection, *EntrainDeep*, acts much like that for shallow convection in terms of the radiation budget, with the important difference that the low-level cloud cover increase with increasing *EntrainDeep* is to some extent compensated by loss of high-level ice clouds. Increasing *EntrainDeep* also increases lower- and middle-tropospheric water vapour because more water is mixed into the free troposphere instead of being transported higher where it would be converted to rain. Associated with convective transport of humidity is a cooling of the upper troposphere due to evaporation on the one hand, and radiative warming from the formation of cirrus clouds on the other hand.

A fourth parameter, *AutoConversion*, describes the conversion rate of cloud water to rain in convective systems. Increasing *AutoConversion* reduces cloud cover and atmospheric water vapour. Both TOA short-wave and long-wave irradiance change with *AutoConversion*, but because the short- and long-wave changes are in opposite direction, the TOA radiation budget is less affected.

The remaining parameters describe the mountain lift forces through orographic gravity waves (*OroLift*), and oceanic vertical mixing (*OceanMixBack, OceanMixRich, OceanMixEddy*). *OroLift* corresponds to the parameter C_l in Eq. (4) of Lott (1999) and affects the magnitude of northern midlatitude wind stress. *OceanMixBack* governs the background vertical diffusivity, *OceanMixRich* enters the Richardson number dependent term in the equation for the vertical diffusivity coefficient (Pacanowski and Philander, 1981), and *OceanMixEddy* affects the mixing of tracer by advection from unresolved oceanic mesoscale eddies parametrized after Gent *et al.* (1995). As the impact of these parameters on the atmospheric circulation and TOA radiation budget is weak, they will not be discussed further in this article.

To understand the spread of pre-industrial climates which is sampled by the 66 model configurations, an energy balance model is used (Heinemann *et al.*, 2009; Voigt *et al.*, 2011). In terms of incoming solar and outgoing long-wave radiation, the surface temperature is given by

$$S(1-\alpha) = \epsilon\sigma T^4, \tag{1}$$

where S is the downward solar irradiance at the TOA, α the planetary albedo, σ the Stefan–Boltzmann constant, ϵ the effective emissivity, and T the surface temperature. The effective emissivity and the planetary albedo are calculated using radiative fluxes from the different simulations. The energy balance model adequately describes the temperature spread, as is illustrated by the grey dots in Figure 1.

The short-wave cloud-radiative effect can be identified as the factor that explains most of the temperature spread. To see this, all terms in Eq. (1) except one are taken from the pre-industrial climate of the standard configuration, while one term is diagnosed from the respective model configuration. Figure 1(a) shows that the temperature spread is largely due to the spread in planetary albedo; open circles indicate the temperature difference calculated in the energy balance model when the planetary albedo is taken from the model configuration under investigation while all other terms Eq. (1) have the values of the standard configuration. The planetary albedo is due to the effect of both clouds and surface albedo. Because surface albedo differences are relatively small across the configurations (see above), differences in the cloud short-wave radiative effect carry most of the temperature spread (Figure 1(b)). The range of the clear-sky albedo explains only about a quarter of the temperature spread; effective emissivity exhibits a large scatter across the configurations with no distinct explanatory feature (not shown).

In the next section we explore the connection between these differences in clouds and the large-scale tropical circulation.

3. Clouds and tropical circulation

The previous section established that clouds are the primary source of the temperature spread across the model configurations. Now we establish how moisture and cloud cover relate to the strength of the tropical circulation.

3.1. *The tropical circulation*

We use the mean-meridional mass streamfunction to measure the strength of the tropical circulation. While computing the streamfunction is straightforward, some care is needed in its interpretation. Because of nonlinear seasonal variations in

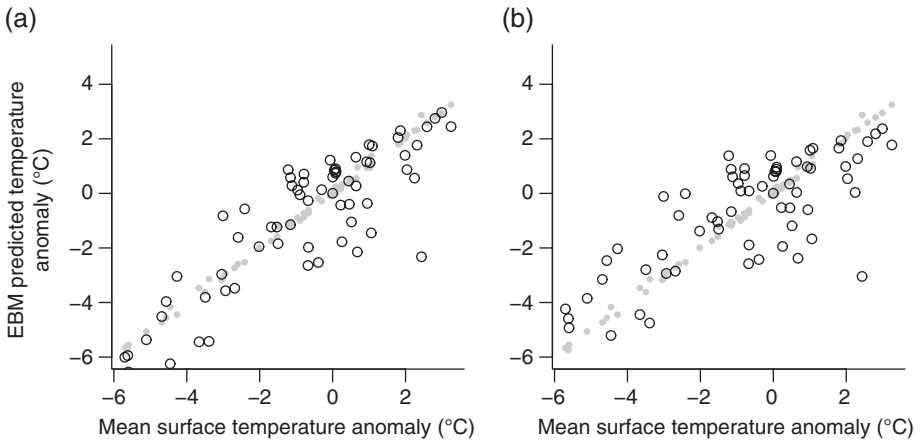

Figure 1. Open circles indicate the contribution of (a) planetary albedo and (b) short-wave cloud radiative effect to the differences in global mean temperature across the model configurations. Grey dots show the differences between the surface temperature of the standard configuration and the perturbed configuration versus the same global mean surface temperature differences as predicted by the energy balance model through Eq. ((1).

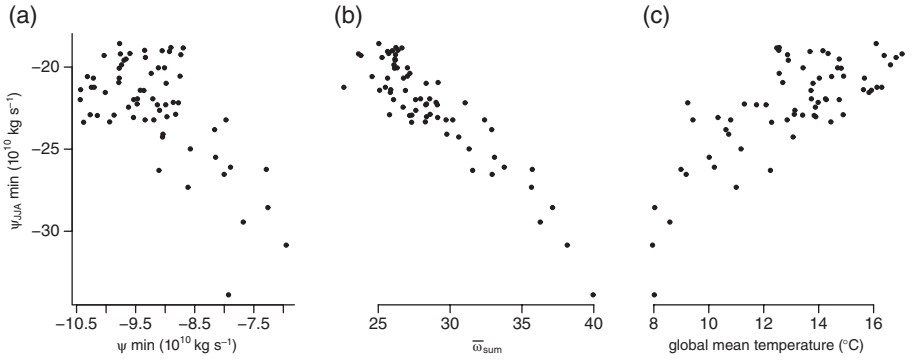

Figure 2. (a) Scatter plot of minima of the time mean mass streamfunction versus JJA seasonal mean mass streamfunction minima. (b) Minimum of the JJA mass streamfunction against $\bar{\omega}_{\rm sum}$. (c) Minimum of the JJA mass streamfunction against global mean temperature.

the streamfunction, the annual-mean streamfunction shows the opposite characteristics to the seasonal-mean streamfunction; the latter being calculated for June-July-August (JJA, Figure 2(a)). Colder climates have shallower and weaker annual streamfunctions but stronger seasonal streamfunctions than warmer climates (Figure 2(c)).

The seasonal and not the annual-mean streamfunction is the appropriate measure for the strength of the tropical circulation. This can be clearly shown by analyzing the probability distribution P_ω of the tropical monthly-mean vertical pressure velocity at 500 hPa, ω (Bony *et al.*, 2004). We define the edge of the Tropics as those two poleward northern and southern latitudes for which the tropical cells of the mass streamfunction become zero at 500 hPa. The difference in the mean vertical velocities of the subsidence ($\omega > 0$) and convective regions ($\omega < 0$),

$$\overline{\omega}_{\rm sum} = \int_0^\infty \omega\, P_\omega {\rm d}\omega \; - \int_{-\infty}^0 \omega P_\omega \, {\rm d}\omega, \tag{2}$$

yields a commonly used measure for the strength of the tropical circulation (e.g. Vecchi and Soden, 2007). This measure agrees well with the strength of the tropical circulation measured by the JJA streamfunction minima (Figure 2(b)). In the remainder of the article we will use JJA streamfunction minima to express the strength of the tropical circulation, keeping in mind however the equivalence of this measure to $\overline{\omega}_{\rm sum}$.

Colder climates exhibit a stronger tropical circulation, in agreement with Schneider *et al.* (2010) (Figure 2(c)). This feature is also illustrated in more detail in Figure 3 which displays JJA streamfunction composites for the five coldest and the five warmest pre-industrial simulations.

This leads one to wonder what controls the strength of the tropical overturning circulation across the model configurations. A useful starting point to address this question is the fact that in cloud-free tropical regions, such as free-tropospheric subsidence regions, the dominant temperature balance at a fixed pressure level is, up to a pressure-dependent constant (Sobel and Bretherton, 2000),

$$\frac{\partial \theta}{\partial p}\omega \propto Q_{\rm r}\,. \tag{3}$$

Here, θ denotes potential temperature, and $Q_{\rm r}$ radiative cooling. Equation (3) shows that subsidence velocities are tied to the vertical temperature gradient.

In a warmer climate, one generally expects a slowdown of the tropical circulation. The moist adiabatic lapse rate decreases with increasing temperature, and this decrease is communicated from the convective into the subsidence regions due to the smallness of the Coriolis parameter. As a result the absolute value of $\partial\theta/\partial p$ increases such that a smaller ω is sufficient to balance the approximately constant radiative cooling.

However, the temperature dependence of the moist adiabat is not the only reason for the weaker tropical circulations in warmer model configurations. The strength of convective mixing, which differs between the model configurations due to the change in convective parameters, contributes by affecting the vertical temperature profile. Here, and in the reminder of the article, the term 'convective mixing' refers to vertical mixing in the atmosphere due to convective processes. Warmer model configurations happen to exhibit stronger convective mixing (cf. section 5), which leads to a more stable atmosphere and hence weaker circulation. This is illustrated by Figure 4 which shows profiles of moist static energy and saturated moist static energy for a cold configuration with strong circulation, and a warm climate with weak circulation. In the subsidence region, saturated moist static energy increases with height for the weak circulation but is uniform for the strong circulation implying

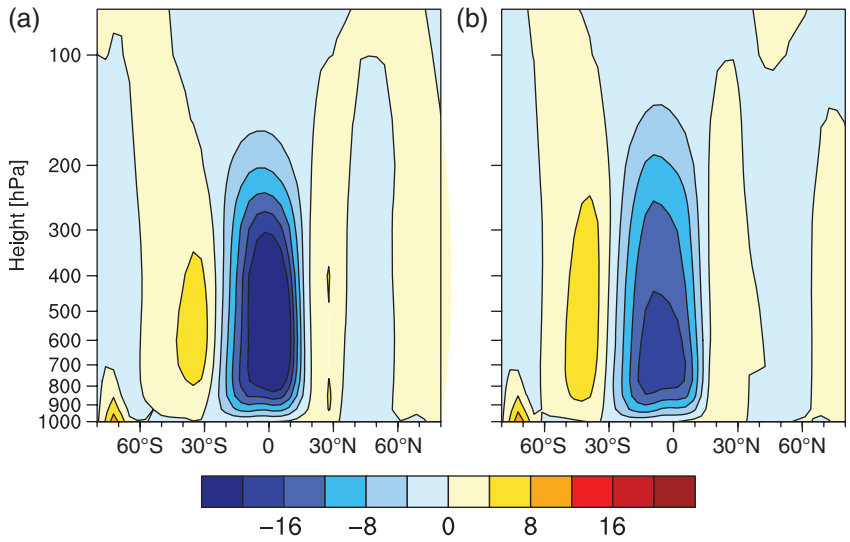

Figure 3. Composites of the June–July–August (JJA) mass streamfunction in units of $10^{10}\,\mathrm{kg\,s^{-1}}$ for (a) the five coldest and (b) the five warmest pre-industrial simulations.

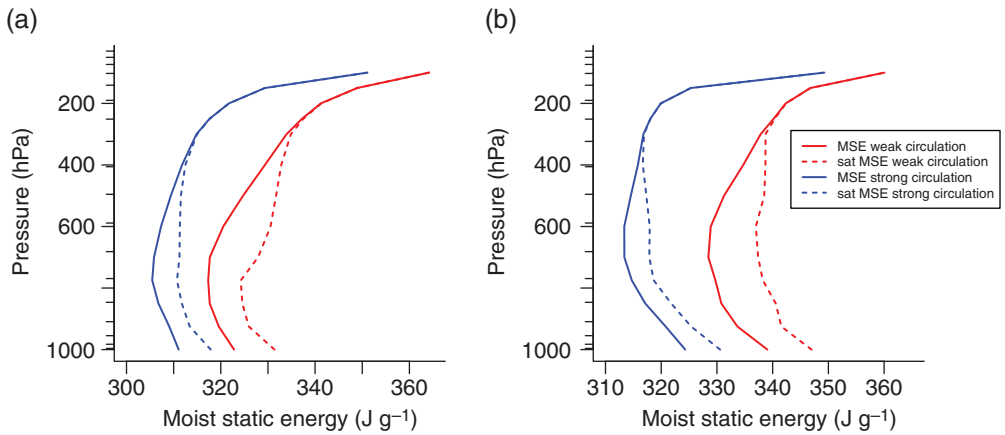

Figure 4. Profiles of moist static energy (solid lines) and saturated moist static energy (dashed lines) of a climate with strong Hadley cell (blue lines), and of a climate with weak Hadley cell (red lines). The zonally averaged JJA zonal mean profile is averaged over (a) the main subsidence region of 15°S to 25°S, and (b) the deep Tropics (5°N to 5°S). The minor tick marks on the *y*-axis indicate the mean model level pressures except for the top one at 10 hPa.

that the more stable stratification in the weak-circulation case is not simply a temperature effect (Figure 4(a)). One can also see analogous differences in the profile of saturated moist static energy in the convective region (Figure 4(b)) that implies more convective mixing in the warm weak-circulation configuration.

The circulation differences could, in principle, also be driven by meridional temperature gradients. Emanuel (1995) discusses the role of horizontal gradients in subcloud-layer equivalent potential temperature (denoted by θ_e) for the onset and control of tropical circulations such as the Hadley, Walker, and monsoon circulations. However, it is important to note that his discussion assumes a perfect moist adiabatic lapse rate, while in global climate models the tropical temperature profile to some extent depends on the characteristics of the convection scheme.

That the vertical and not meridional temperature gradient is the dominant driver of the circulation differences is clearly shown in Figure 5. Figure 5(a, b) show scatter plots of the minima in the JJA mass streamfunction in dependence of the JJA meridional θ_e

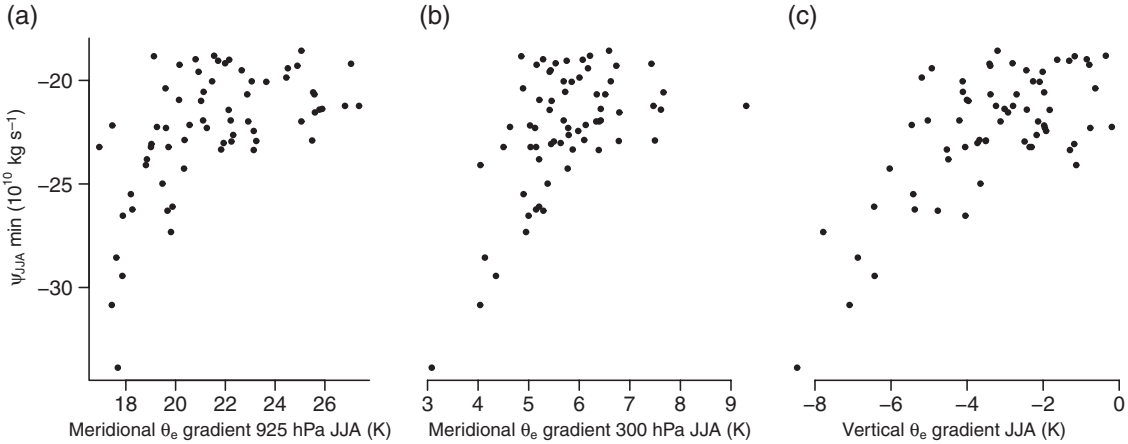

Figure 5. Scatter plots of the minima of the JJA mass streamfunction against JJA meridional θ_e gradients at (a) 925 hPa and (b) 300 hPa. (c) shows the seasonal JJA vertical θ_e gradient, computed as the difference of zonal mean θ_e at 300 and 1000 hPa in the main convective region of the tropical circulation at 11°N.

gradient evaluated at 925 and 300 hPa. The meridional gradient is calculated as the zonal-mean θ_e difference at 11°N and 22°S as these two latitudes roughly correspond to the poleward edges of the streamfunction (Figure 2). In both the subcloud layer as well as in the upper branch of the Hadley cells, the meridional θ_e gradient decreases with increasing strength of the Hadley circulation. Thus, differences in the meridional θ_e gradients are rather the consequence, and not the driving force, of differences in the circulation strength. Instead, the circulation strength is strongly related to the vertical stability of the tropical atmosphere (Figure 5(c)). The less stable the atmospheric column, the stronger is the circulation.

Frierson (2007) offers a framework to interpret the impact of convective mixing on the strength of the tropical circulation. The framework relies on the concept of gross moist stability (Neelin and Held, 1987) that is defined as the amount of energy transported per unit mass transport (Frierson, 2007). If one assumes that the purpose of the tropical circulation is to flatten meridional temperature gradients, then a large gross moist stability implies that a weak circulation is sufficient to transport enough energy poleward. In the opposite case of a small gross moist stability, the circulation needs to be stronger to achieve the same level of energy transport and reduction of meridional temperature gradients.

Figure 6(a) shows the JJA mass streamfunction minimum at the Equator against the JJA northward atmospheric energy transport across the Equator. Seasonal atmospheric energy storage is small and is neglected in the calculation. The fact that stronger circulations achieve less transport implies that they also have a smaller gross moist stability, and that the differences in the circulation strength can thus be understood to result from differences in gross moist stability. Indeed, this is not surprising as gross moist stability is closely connected to the vertical θ_e gradient shown in Figure 5. Both quantities are strongly controlled by the strength of the convective mixing, which indicates that in climate models convective mixing exerts a dominant influence on the tropical circulation to such a degree that meridional temperature gradients are a mere consequence of the strength of the large-scale overturning circulation. Although not considering the impact of eddy momentum transport (Schneider, 2006), our results demonstrate the crucial role that convective mixing plays for the tropical circulation, a process that global climate models can not represent explicitly but need to parametrize. We will argue below that this has also consequences for many other aspects of the tropical circulation.

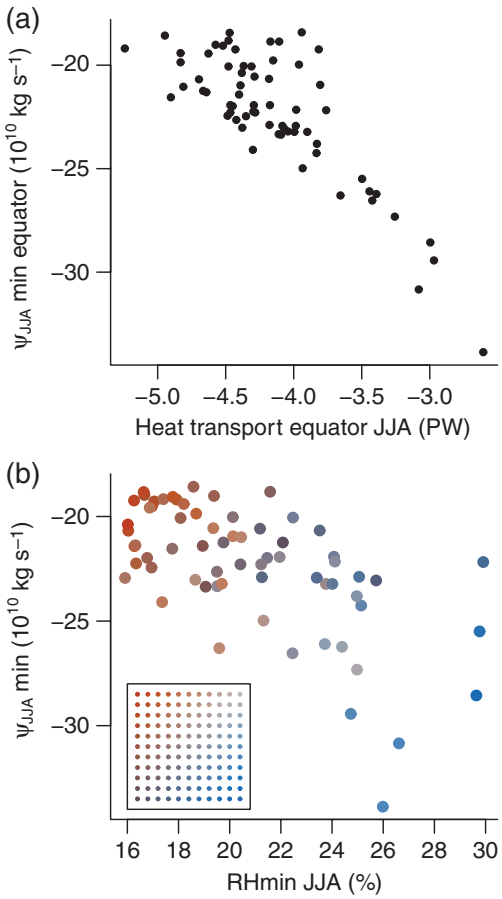

Figure 6. (a) JJA mass streamfunction minimum at the Equator versus JJA northward atmospheric energy transport across the Equator. (b) JJA mass streamfunction minimum versus zonal mean JJA relative humidity minimum over a box which comprises the 400 and 500 hPa level and the latitudes from 9 to 32°S. The dots are coloured according to the corresponding values of *EntrainDeep* and *AutoConversion* (section 4 gives details). The box in the lower left corner shows the colour scheme.

3.2. *Moisture and clouds*

Although it might be expected that a stronger tropical overturning leads to less cloud cover in subtropical dry zones, the model configurations show the opposite effect. Weaker circulations are connected with drier middle tropospheres, especially in subtropical subsidence regions (Figure 6(b)).

The feature that drier mid-tropospheric conditions come with less cloud cover is not confined to regions of large-scale subsidence. Climates with a weak circulation (Figure 7(b)) show a much drier mid-troposphere and reduced cloud cover throughout the Tropics compared to climates with a strong circulation (Figure 7(a)). There are also indications of increased cloud cover around the Intertropical Convergence Zone (ITCZ), both in very high clouds near the tropopause and very low clouds at the top of the boundary layer for climates with a strong circulation, a signature that is indicative of increased deep convective mixing. Mainly in the subtropics and over land in the central ITCZ region, total cloud cover is strongly reduced in configurations with weak tropical circulation (Figure 7(c)). Only oceanic areas in the centre of the ITCZ show larger total cloud cover.

Thus, in the present ensemble, strong deep convective mixing stabilizes the atmosphere in the central ITCZ region leading to a weak tropical overturning circulation and a strong transport of moist and warm boundary-layer air to the upper troposphere where a large portion of the moisture precipitates out. Consequently, simulations with stronger deep convective mixing exhibit drier mid-tropospheric conditions and less cloud cover throughout the Tropics. The reduced cloud cover implies higher surface temperatures.

In the next section, we further substantiate the established connection between convective mixing, the strength of the tropical circulation, and atmospheric moisture by a parameter regression analysis.

4. The role of the parameters

After having studied the connections between a number of important elements of the tropical atmosphere and having built physical understanding of these connections, we now turn to the varied parameters. We perform a regression analysis to relate the parameters to the climate characteristics of the model configurations to identify the parameters, and associated processes, that lead to these connections. The regression analysis is restricted to the atmospheric convection parameters *CloudOvershoot*, *EntrainShallow*, *EntrainDeep*, and *AutoConversion*.

Global mean temperature, JJA mass streamfunction minimum, and JJA relative humidity minimum of the model configurations are regressed against the parameters to understand the climatic effect of the latter. The results are summarized in Table 2 in terms of explained variance increases for each step in the regression. Before the regression analysis is performed, the parameters *EntrainDeep*, *EntrainShallow*, and *AutoConversion* are

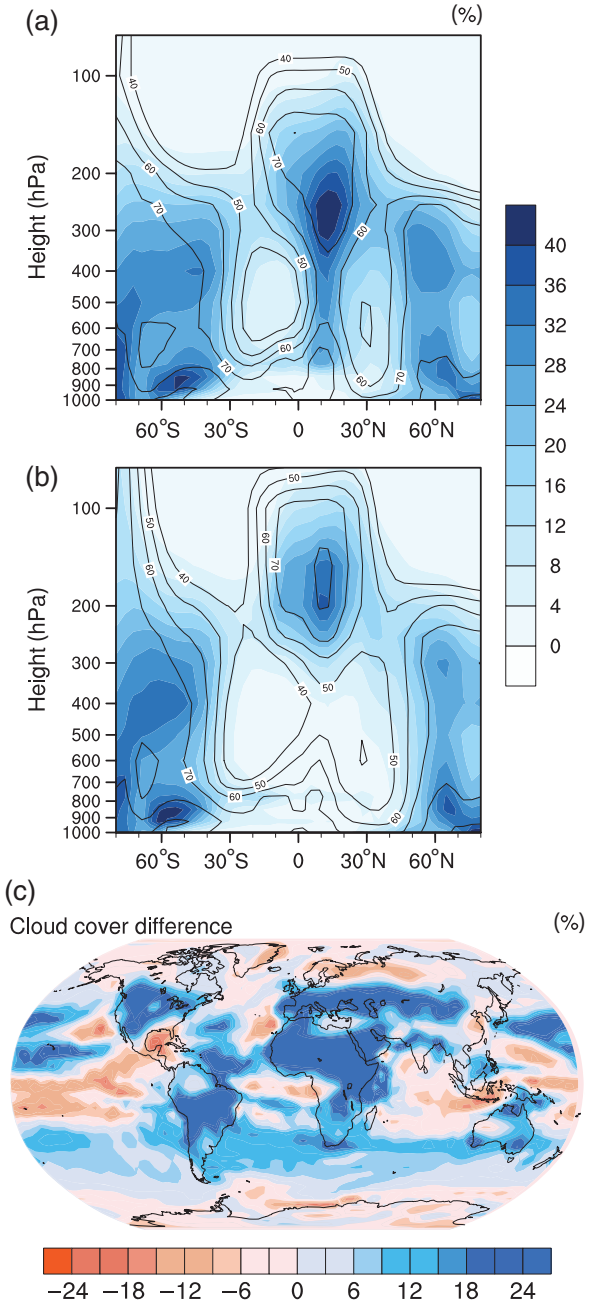

Figure 7. Composites of zonal mean JJA cloud cover computed using (a) the five model configurations with the strongest tropical circulation, and (b) the five model configurations with the weakest tropical circulation. Contour lines indicate relative humidity. (c) shows differences in JJA cloud cover between the simulations with strong tropical circulation and those with weak tropical circulation.

transformed to their logarithmic values, and all parameters are normalized by their respective standard deviations.

For global mean temperature, only *EntrainDeep*, *EntrainShallow*, and *CloudOvershoot* enter the regression. The inclusion of the parameter *AutoConversion* does not increase the explained variance, and the corresponding regression coefficient is not significantly different from zero. The entrainment rate for deep convection explains most of the variance, namely 42.5%. Smaller values of the entrainment rate of both deep and shallow convection lead to a higher temperature. *CloudOvershoot* is positively correlated with global mean temperature.

For the strength of the tropical circulation, the entrainment rate for deep convection again explains most of the variance, namely 65%. If one includes the entrainment rate for deep convection in the regression, then *CloudOvershoot* becomes insignificant. Therefore, the regression only uses *EntrainDeep*, *EntrainShallow*, and *AutoConversion*. Smaller entrainment rates for both deep and shallow convection lead to weaker circulations. The reason for weaker circulation with more deep convective mixing (i.e. less lateral entrainment of environmental air or, equivalently, smaller values of *EntrainDeep*) was discussed in section 3.1. For *EntrainShallow*, the shallow cumulus humidity throttle mechanism (Neggers *et al.*, 2007) might play a role, though the effect of *EntrainShallow* on the circulation strength partly results from the fact that the shallow cumulus parametrization in some conditions takes over convective events that indeed become deep. A smaller value of *AutoConversion* leads to a stronger circulation, but the explained variance only increases by 1.1%.

For the JJA relative humidity minimum, only *EntrainDeep*, *EntrainShallow*, and *AutoConversion* are used. As before, *EntrainDeep* explains most of the variance, namely 54.6%. Smaller values of *EntrainDeep* lead to drier conditions, in line with the arguments presented in section 3. *AutoConversion* is the second most important parameter, and in a single variable regression explains 40.3% of the variance. In the stepwise regression that includes both *EntrainDeep* and *AutoConversion*, the explained variance is 84.7%. Additionally including *EntrainShallow* further increases the explained variance to 87.1%. The inclusion of *CloudOvershoot* does not increase the explained variance, and the corresponding regression coefficient is not significantly different from zero during any step of the regression analysis.

The colour scheme for the dots in Figure 6(b) illustrates the results of the regression analysis in the cases of the strength of the JJA mass streamfunction and the JJA relative humidity minimum. Dark grey colours correspond to dots for which both *EntrainDeep* and *AutoConversion* are small, light grey colours correspond to dots for which both *EntrainDeep* and *AutoConversion* are large. Red colours indicate dots for which *EntrainDeep* is small and *AutoConversion* is large, and vice versa for blue coloors.

In summary, the regression supports our previous findings. *EntrainDeep*, the parameter related to deep convective mixing, is the main control on strength of the tropical circulation, global mean temperature and mid-tropospheric relative humidity. *EntrainShallow*, the entrainment rate of shallow convection, plays a minor role. However, it should be noted that the latter is potentially due to a deficiency in how the version of ECHAM6 applied here represents the interaction between the convection scheme, the cloud cover scheme, and the large-scale condensation scheme. We will return to this point in section 5.2. The other main convective mixing parameter, *CloudOvershoot*, has little effect on the dynamics and large-scale humidity, but influences cloud cover and thus global mean temperature. Finally, the conversion rate of cloud water to rain, *AutoConversion*, does not affect global mean temperature and the strength of the tropical circulation, but impacts cloud cover and the moisture content of the atmosphere.

Table 2. Increases in explained variances due to stepwise inclusion of the parameters in a stepwise regression analysis for global mean temperature, JJA mass streamfunction minimum, and JJA relative humidity minimum. A plus sign indicates a positive correlation of the parameter with the regressed variable, a negative indicates a negative correlation.

Regression step	Global mean temperature		JJA Ψ_{min}		JJA RH_{min}	
First	*EntrainDeep*:	42.5% −	*EntrainDeep*:	65.0% −	*EntrainDeep*:	54.6% +
Second	*CloudOvershoot*:	22.0% +	*EntrainShallow*:	11.3% −	*AutoConversion*:	30.1% −
Third	*EntrainShallow*:	13.3% −	*AutoConversion*:	1.1% +	*EntrainShallow*:	2.4% +

5. Climate sensitivity

The previous analysis established a close connection between the large-scale tropical circulation and parameters related to the representation of convection, parameters which in one fashion or another determine the degree of convective mixing. Less entrainment by deep convection favours deeper and more adiabatic deep convective updraughts, which results in a more stable atmosphere throughout the Tropics, and weaker overturning. Because turbulent entrainment and turbulent detrainment are equal (except at cloud top) in the convection scheme, with a small value of turbulent entrainment/detrainment more water is precipitated and less is mixed laterally. This process is consistent with a drier lower and middle troposphere in the climates with more thermal stratification and a weaker circulation, e.g. Figure 7. In the following it will be shown that the manner in which convection mixes the tropical troposphere also has a strong influence on the equilibrium climate sensitivity (ECS).

The ECS from the simulations is calculated using a regression technique, following Gregory *et al.* (2004). Because the simulations over which the regression is based are for a quadrupling of atmospheric carbon dioxide, the resultant temperature is divided by two, to be consistent with the temperature response one expects for a doubling of atmospheric carbon dioxide. For most of the simulations, this is a good approximation, but three of the simulations have a very high climate sensitivity and are still far from equilibrium at the end of the 150 year simulation period. For these simulations there is evidence of substantial nonlinearity in the regression. Repeating the regressions using the surface, rather than the TOA, energy balance also shows a nonlinear response, suggesting that it is not an artifact of state-dependent energy leakages in the atmosphere (e.g. Stevens *et al.*, 2013). Hence, for these high-sensitivity configurations, the estimates of the ECS are uncertain. Therefore, in subsequent analysis, the ECS of these simulations is set to 10 °C. Although so doing underestimates the ECS of these simulations, this limit is chosen so as to avoid having a few simulations unduly influencing the regression. This is a somewhat arbitrary choice, and will somewhat degrade the explained variance in the regression analysis, but qualitatively the result does not depend on the specific assumed climate sensitivities for these very-high-sensitivity configurations of the model. The remaining simulations have an ECS between 3 and 8 °C. Given experiences with higher-resolution versions of the same model, whose ECS is nearer 3.5 °C (Stevens *et al.*, 2013), the absence of configurations with an ECS less than 3 °C is surprising, as are the overall large values.

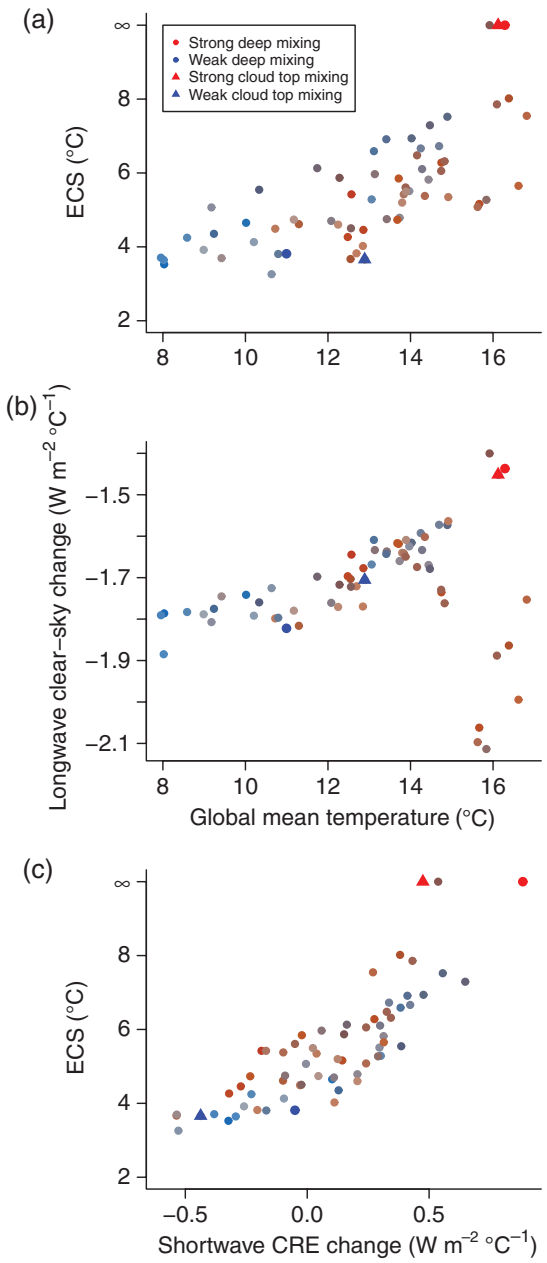

Figure 8. (a) Climate sensitivity of the different climates versus global mean temperature. (b) Slopes of the regression lines when clear-sky outgoing long-wave radiation anomalies are regressed against global mean temperature anomalies in the 'abrupt 4×CO_2' experiments. (c) is as (b), but with short-wave cloud radiative effect (CRE). The colour shading of the dots is as in Figure 6.

5.1. *Relation between ECS and indicators of the large-scale state*

The ECS and the global mean temperatures of the perturbed physics ensemble correlate reasonably well with one another (Figure 8). However, the correlation is not strong enough to meaningfully constrain the ECS based on knowledge of the present temperature, as for any given globally averaged temperature a wide range of climate sensitivities is sampled.

A null hypothesis would be that the differences in global mean temperature across the ensemble *per se* imply the differences in ECS. Meraner *et al.* (2013) noted a relation between ECS and global mean temperature in the MPI-ESM-LR, a slightly higher-resolution version of the same model. They argued that this sensitivity resulted from an increase in water vapour feedback associated with a rising tropopause height. Figure 8(b) shows the slopes of regression lines when clear-sky outgoing long-wave radiation anomalies are regressed against global mean temperature anomalies in the various 'abrupt 4×CO_2' experiments. These slopes are good proxies for joint water vapour and temperature feedbacks. The decrease in long-wave clear-sky feedback accounts for some of the spread in model climate sensitivities, but for some warm climates it even drops. This shows that the spread in ECS does not predominantly result from spread in the long-wave feedback, which implies that stratospheric water vapour likely plays a minor role in our perturbed physics ensemble (Joshi *et al.*, 2010). Overall the range in simulated climate sensitivities in the present simulations are more closely linked to differences in short-wave cloud radiative effect (CRE) changes (Figure 8(c)), indicative of a more important role for short-wave cloud feedbacks across the ensemble (e.g. Vial *et al.*, 2013). Hence, parameter changes that affect climate sensitivity, through their influence on cloud feedbacks, also likely control the global mean temperature in the control climate, through their influence on the distribution of clouds.

In an analysis of a multi-physics ensemble taken from the CMIP suite of experiments Fasullo and Trenberth (2012) reported a relationship between ECS and the seasonal, JJA, subtropical relative humidity minima, $RH_{\min}$, and the streamfunction minima, $\Psi_{\min}$, respectively. The relationship between ECS and both $RH_{\min}$ and $\Psi_{\min}$ are shown with the help of Figure 9. These relationships are not as pronounced as the relationship between globally averaged surface temperature and ECS.

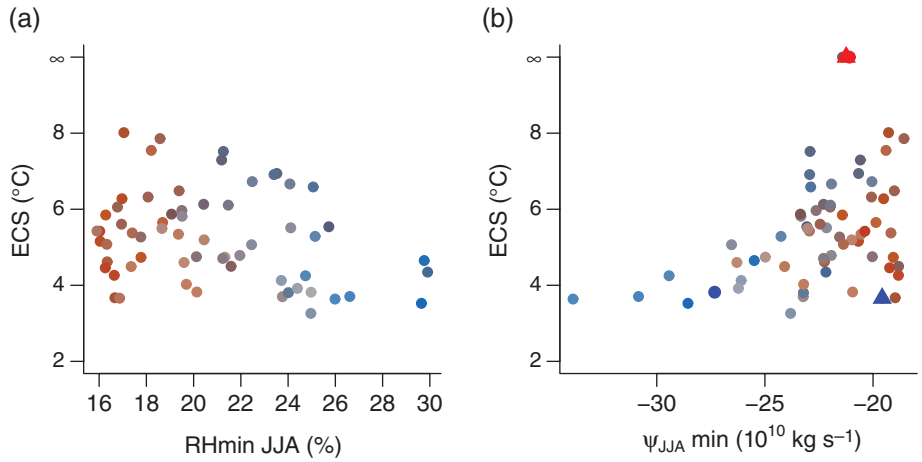

Figure 9. (a) Zonal mean JJA seasonal relative humidity minima (as in Figure 6) versus climate sensitivity. (b) JJA mass streamfunction minima versus climate sensitivity. The colour shading of the dots is as in Figure 6.

An argument for the correlation between the relative humidity of the base climate and the climate sensitivity can be developed from a consideration of the bulk boundary-layer moisture budget over tropical oceans away from regions of deep convection. In stationarity and in the absence of evaporating precipitation, the boundary-layer moisture budget takes the following form:

$$\nu_{\rm srf}(q_{\rm srf} - q_{\rm bl}) + \nu_{\rm entr}(q_{\rm ft} - q_{\rm bl}) = 0\,, \qquad (4)$$

where $q_{\rm bl}$, $q_{\rm ft}$ and $q_{\rm srf}$ are the total water content of the boundary layer, the free troposphere, and the surface moisture availability, respectively, and $\nu_{\rm srf}$ and $\nu_{\rm entr}$ are velocity scales for the surface exchange and mixing across the top of the boundary layer (Stevens, 2006, gives details). In the present context $\nu_{\rm entr}$ measures lower tropospheric mixing.

Solving Eq. (4) for $q_{\rm bl}$ and taking the partial derivative of $q_{\rm bl}$ with respect to $\nu_{\rm entr}$ gives

$$\frac{\partial q_{\rm bl}}{\partial \nu_{\rm entr}} = \frac{\nu_{\rm srf}}{(\nu_{\rm entr} + \nu_{\rm srf})^2}(q_{\rm ft} - q_{\rm srf}), \qquad (5)$$

i.e. the susceptibility of the boundary-layer moisture content to changes in the entrainment of dry, free-tropospheric air is proportional to the difference in the moisture content of the free troposphere and the near-surface layer. Related arguments implying a stronger, or more effective, lower-tropospheric mixing underlie the physical mechanisms for a positive low-cloud feedback in the work of Brient and Bony (2012) and Rieck *et al.* (2012), and is used to explain the correlation between lower-tropospheric mixing and the ECS in a recent study by Sherwood *et al.* (2014). Here we attempt to relate the argument to the tropospheric humidity directly by suggesting that a given increase in the mixing between the boundary layer and free atmosphere (as measured by $\delta\nu_{\rm entr}$) in a drier atmosphere will cause more drying of the boundary layer, and thus implies a larger climate sensitivity.

These arguments notwithstanding, the physical correlation between $RH_{\rm min}$ and ECS is not pronounced, e.g. Figure 9. Because the convective mixing parameters are what is varied in the simulations, the degree to which the JJA $RH_{\rm min}$ fails to correlate with ECS suggests that it is a poor indicator of those aspects of convective mixing which are important for the climate sensitivity of the different ECHAM6 configurations. Moreover, the lack of a strong correlation between ECS and $RH_{\rm min}$ and, if anything, a weak negative correlation between ECS and $\Psi_{\rm min}$, indicates that the explanatory framework proposed by Fasullo and Trenberth (2012) is not robust.

5.2. *Parameter regression*

To quantitatively explore the relative role of the parameters in determining the climate sensitivity, a linear regression analysis is performed. Following the methodology introduced in section 4, the regression analysis is based on the transformed and normalized parameters. In a single-parameter regression, *EntrainDeep* explains most of the variance of climate sensitivity, namely 23.2%. *AutoConversion* and *CloudOvershoot* explain 8.8% and 1.8% of the variance respectively. *EntrainShallow* is not significant. The turbulent entrainment/detrainment rate of deep convection is thus the most important variable not only in controlling the structure of the base climate, but also in determining the ECS.

The apparent importance of secondary parameters is influenced by how one performs the regression, as a multi-parameter regression identifies a larger role for the secondary parameters. Including both *EntrainDeep* and *AutoConversion* in the regression explains about 5% more variance than they explain individually (Table 3). More importantly, adding *CloudOvershoot* to *EntrainDeep* and *AutoConversion* increases the explained variance from 37.2% to 55.2%, enhancing its importance by about a factor of ten compared to a single-parameter regression, which makes it almost as important as *EntrainDeep*. Although in the multi-parameter regression the effect of *EntrainShallow* becomes significant, it still increases the explained variance by only a small (4.1%) amount. This analysis demonstrates that the single-variable regression generally understates the role of secondary parameters, and can be misleading.

The ways in which the three dominant parameters correlate with ECS is not entirely consistent with the way in which they correlate with major features of the tropical circulation, as presented in Table 2. For instance, although the sign of the correlations of *CloudOvershoot* and *EntrainDeep* and ECS are consistent with co-variability between the globally averaged surface temperature and the ECS, *EntrainShallow* is important for the globally averaged surface temperature, but not the ECS. And although the seasonal minimum in relative humidity in the base climate is positively correlated with *EntrainDeep* and negatively correlated with *AutoConversion*, the correlation of the ECS with *AutoConversion* and *EntrainDeep* has the same sign (Table 3). This result further suggests that attempts to relate the ECS to the dryness of the lower-middle troposphere are not likely to be as robust, as for instance suggested by Fasullo and Trenberth (2012) on the basis of results from a multi-model ensemble. In the case of the present ensemble, the main reason for the fact that climates with rather moist atmospheres can exhibit very high climate sensitivities is associated with the role of the *AutoConversion* parameter. This role is discussed in more detail using the example of one of the very high sensitivity model configurations in section 5.3, but it also becomes apparent from the colour shades in Figures 8 and 9. High climate sensitivity configurations are typically related to dark greyish or brownish colours which means small values for both *EntrainDeep* and

Table 3. Percent variance in climate sensitivities explained (and sign of correlation) by the three most important parameters in single- and multi-parameter regressions.

Parameter	Single	Multi	Sign
EntrainDeep	23.2	23.2	−
AutoConversion	8.8	14.0	−
CloudOvershoot	1.8	18.9	+

AutoConversion. However a small value of the *AutoConversion* parameter leads to a relatively moist atmosphere, counteracting the drying tendency coming with a small value for *EntrainDeep*.

The limited influence of *EntrainShallow* is surprising, given the analysis by Sherwood *et al.* (2014), in which shallow mixing correlates much more strongly with the spread of climate sensitivities in two generations of CMIP models. However we believe that, due to deficiencies in the implementation of the cloud parametrization used in the present version of the ECHAM (cf. Stevens *et al.*, 2013), *EntrainShallow* exerts less of a control on shallow mixing than one would initially suspect. This is confirmed by simulations with a more recent development version of ECHAM, in which the implementation deficiencies were resolved, and in which *EntrainShallow* does have a much stronger impact on climate sensitivity (T. Mauritsen, 2014; personal communication), more in line with the results presented by Sherwood *et al.* (2014).

5.3. *Comparing divergent configurations*

To get further insight into the role of specific parameters, it proves instructive to pair the configurations with very high climate sensitivities with configurations with much lower values of ECS. Two pairs of simulations are compared, allowing a more detailed inspection of two of the very high sensitivity models. The third large ECS configuration represents a mixture between 'Strong deep mixing' and 'Strong cloud-top mixing' and is not singled out for further study. One pair of configurations selected for further investigation consists of a 'strong deep mixing' configuration with a very large ECS (red circles) and a 'weak deep mixing' configuration (blue circles) with a much smaller ECS (Figure 10(a)). The other pair consists of a 'strong cloud-top mixing' configuration with a very large ECS (red triangles) and a low ECS 'weak cloud-top mixing' configuration (blue triangles, Figure 10(b)). Key parameters distinguishing these four configurations from one another are illustrated relative to the range of parameter values in Figure 10(c, d). The nomenclature implies that 'weak mixing' (blue) models are cooler and characterized by a smaller ECS than the 'strong mixing' (red) models.

The pairs of configurations further substantiate ideas developed, in different ways, in earlier sections. The low ECS configurations are not characterized by a systematically moister lower-middle troposphere, nor are they characterized by a systematically weaker circulation than the high-sensitivity models. This is illustrated in Figure 9, where the configurations with a small ECS span the range of tropospheric humidities and circulation strengths, and the high-sensitivity models are characterized by moderate values of RH_{min}, contrary to the correlations identified by Fasullo and Trenberth (2012) in a multi-model ensemble. Comparing the deep mixing (circle) simulations, it is apparent that the dry troposphere that one might expect from the high-sensitivity model, with small values of deep convective entrainment/detrainment, is offset by small values of *AutoConversion* which supports a relatively more moist JJA subtropical relative humidity minimum (Figure 9(a)) than would otherwise be expected and, given its global mean temperature, rather high total cloud cover.

Zonally averaged changes in relative humidity and cloud cover between the last 20 years of the 'abrupt $4\times CO_2$' simulations and the control simulation of each configuration suggest that the large ECS models are characterized by stronger changes through a deeper tropical overturning simulation than are the small ECS configurations. This is illustrated in Figure 11 for the 'deep mixing' configurations (identified by circles in the previous figures), but similar patterns emerge from a comparison of the cloud-top mixing configurations. Changes in both configurations share some general features, namely an upward and poleward shift in the tropical circulation, as indicated by the horseshoe-like pattern of drying in the tropical upper troposphere, and in the storm tracks. The stratosphere moistens, as do regions in the high latitudes which see more moisture from the poleward shift of the storm tracks. Apart from the more pronounced changes in the high ECS configurations, the drying pattern in the 'weak deep mixing' configuration (Figure 11(a)) is countered by a large region of moistening, and enhanced cloud cover, in the lower and middle troposphere within the Tropics. Such a feature of tropical moistening in the weak ECS models is even more pronounced in the 'weak cloud-top mixing' configuration. The reinforcement of low and mid-level tropical clouds in the low ECS reinforces the pattern of cloudiness that distinguishes the rather cooler models from the rather warmer configurations in Figure 7, consistent with the tendency of cooler models to warm less than the warmer models.

The different pairs of configurations help illustrate the important role of the *AutoConversion* parameter in the deep convection scheme. More *AutoConversion* would be expected to remove water from the troposphere and lead to less cloud. Roughly speaking, the water detrained into the cloud scheme, $q_{\rm cld}$, will be some fraction of the detrained condensed water, $q_{\rm cnd}$, such that

$$q_{\rm cld} \sim (1 - C_{\rm auto})\, q_{\rm cnd}\,, \tag{6}$$

where $C_{\rm auto}$ denotes the *AutoConversion*. Such a relation implies that changes in the condensation rate, for instance associated with a warming climate, will lead to increased amounts of condensed water,

$$\delta q_{\rm cld} \sim (1 - C_{\rm auto})\, \delta q_{\rm cnd}\,, \tag{7}$$

in a way that is modulated by the *AutoConversion* parameter. For a simple cloud model behaving as illustrated, configurations with a smaller value of $C_{\rm auto}$ can support larger changes in cloudiness for a given change in $q_{\rm cnd}$. Likewise, configurations that produce more low-level clouds to begin with can support larger changes in these climatologically important cloud regimes.

A model configuration with a larger value of the *AutoConversion* parameter, 'large rain conversion,' whose parameter values are denoted by the orange symbols in Figure 10(c, d), is illustrative of these points. The values of both *EntrainDeep* and *CloudOvershoot* suggest a high climate sensitivity. But the regression analysis of the corresponding 'abrupt $4\times CO_2$' experiment (Figure 12(a)) suggests a moderate ECS – at least relative to the present ensemble. The initial approach to equilibrium of the warming experiment forebodes a very large (6–7 °C) ECS. But after some warming, the TOA radiative imbalance starts decreasing rapidly without further changes in temperature, so that the final ECS is about 4 °C. The changes from a highly sensitive response to a much less sensitive response after about 6 °C of warming is mostly associated with a change in short-wave CRE, albeit partly offset by accompanying and opposite changes in long-wave CRE. Although one cannot rule out grid-scale effects, for instance associated with circulation features suddenly transitioning to a different level, such a change is consistent with a tendency toward increasing low-level clouds, or a reduction in the decrease of low-level clouds with increasing warming, as might be expected if the tropical atmosphere had dried sufficiently not to support further low-level cloud decreases.

6. Conclusions

A perturbed parameter ensemble is constructed using a coarse resolution version of the MPI-ESM. In addition to a control

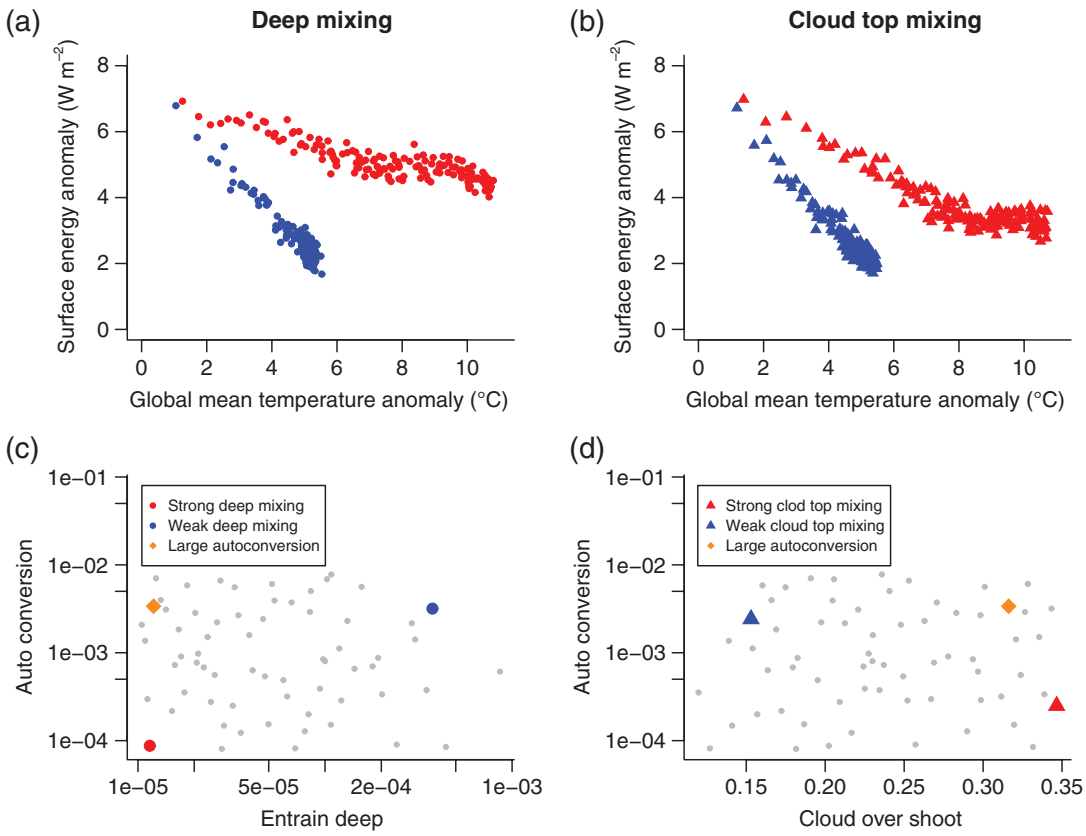

Figure 10. Surface Gregory plots for (a) the 'strong deep mixing' (red dots) and 'weak deep mixing' (blue dots) experiments, and for (b) the 'strong cloud-top mixing' (red dots) and 'weak cloud-top mixing' (blue dots) experiments. Two-dimensional projection of the parameter sample onto the plane defined by (c) the parameters *EntrainDeep* and *AutoConversion*, and by (d) the parameters *CloudOvershoot* and *AutoConversion*.

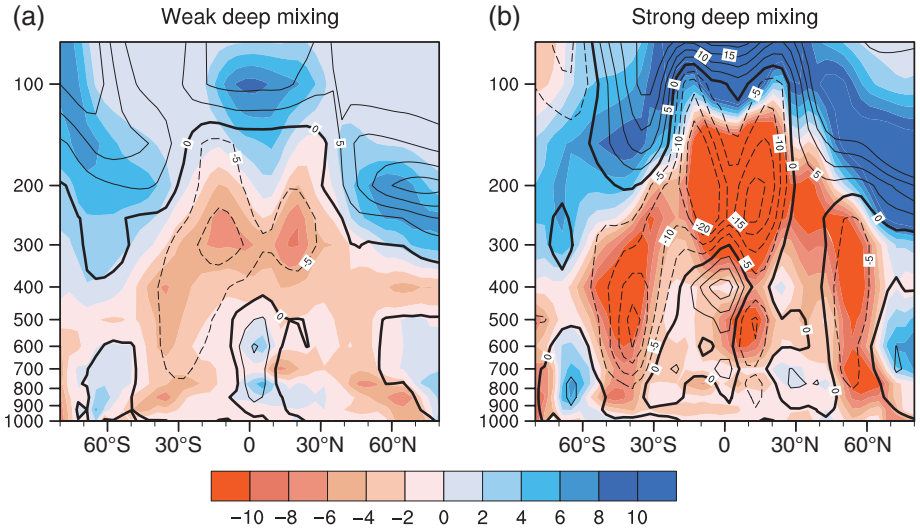

Figure 11. Difference in zonal mean JJA cloud cover between the last 20 years of the 'abrupt $4\times CO_2$' experiment and the pre-industrial climate for (a) the 'weak deep mixing' model and (b) the 'strong deep mixing' configuration. Contour lines indicate relative humidity differences, with dashed contours denoting decreases, and the bold line indicating zero.

configuration, 100 coupled model configurations are constructed by randomly sampling eight parameters used in the component atmosphere and ocean models and thought to be important for the simulated climate and its sensitivity to perturbations. Each configuration is run for 600 years to bring it to a reasonably stationary pre-industrial control state, and then for an additional 150 years after an instantaneous quadrupling of atmospheric carbon dioxide. Of the 101 experiments, 66 are identified as suitable for further study.

Of the parameters that are varied, far and away the most important for the mean climate, and the climate sensitivity, are four parameters related to the convective parametrization. Three of these regulate mixing, for instance by setting the turbulent lateral entrainment (equivalently the detrainment) rate in the deep and shallow convective cloud models used by the convective schemes, or by varying the fraction of the mass flux that is detrained above the level of neutral buoyancy. One parameter affects the rate at which cloud water in the convective updraughts is converted to precipitation. Due to their controlling nature, the effect of these parameters on the base climate, the nature of the large-scale circulation, and on the climate sensitivity is studied further. The convective parameters influence the climate sensitivity and the base climate in different ways, but as a rule less turbulent entrainment by deep convection allows the convective plumes to penetrate deeper, and to maintain the surrounding tropical atmosphere at a greater static stability. The enhanced stability reduces the strength of the overturning circulation, and is associated with tropical circulation whose

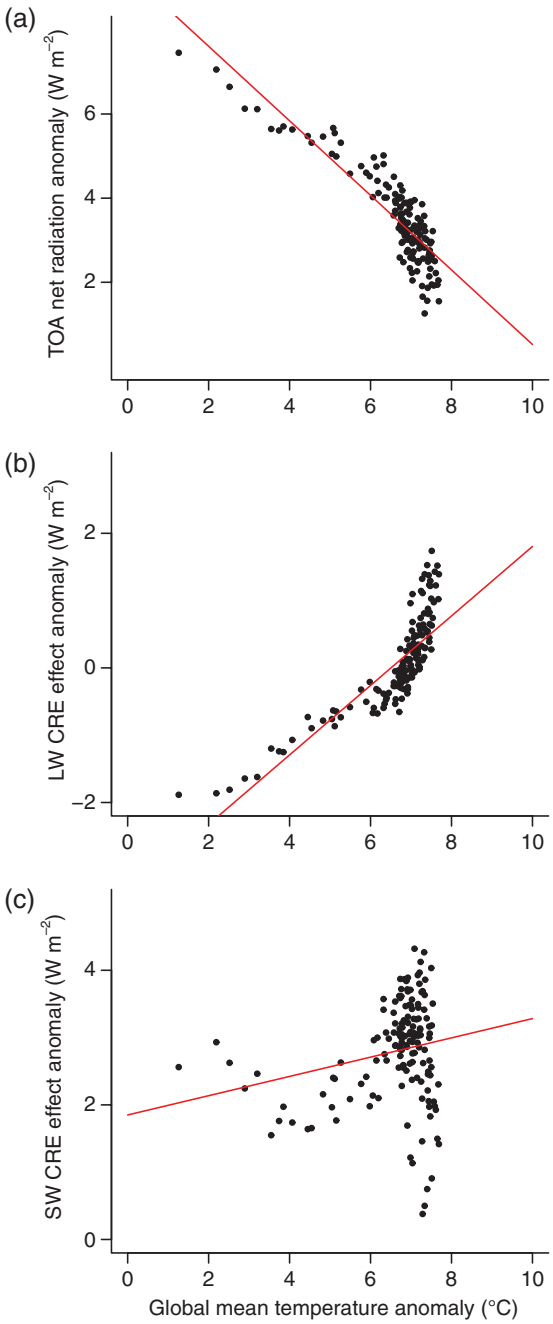

Figure 12. Scatter plot of yearly global mean temperature anomalies against (a) TOA net radiation anomalies, (b) long-wave cloud radiative effect anomalies, and (c) short-wave cloud radiative effect anomalies for the 'large rain conversion' experiment.

subsiding branches are somewhat drier than simulations with more turbulence mixing by convection. Although a great deal of work devoted to understanding the large-scale overturning circulation in the Tropics is related to the controlling influence of external parameters, such as meridional temperature gradients, the simulations show that the choices one makes in formulating convection can play a decisive role in determining the structure of proximate controlling parameters, such as meridional gradients in moist static energy.

The perturbed parameter ensembles samples a wide range of pre-industrial climates, and climate sensitivities. The equilibrium climate sensitivity ranges from about 3 °C to more than 10 °C with evidence of a runaway, or at least very large, warming in three of the 66 model configurations studied. Given that the standard-resolution version of the model has an equilibrium climate sensitivity near the lower end of the range simulated by the perturbed parameter ensemble generated by a coarse resolution version of the same model, the lack of low equilibrium climate sensitivity models is surprising. There is a temptation to take this result as being indicative of high climate sensitivities being more probable, which would agree with the inferences made by Sherwood *et al.* (2014) and Fasullo and Trenberth (2012) on somewhat different grounds. However, given the importance of convective mixing in the lower tropical troposphere to the climate sensitivity, and being cognizant of the fact that it arises from poorly understood interactions of admittedly crude representations of convective processes through the depth of a troposphere that is not well resolved, one hesitates to jump to such a conclusion. Given that climate models tend to underestimate entrainment of environmental air in deep convective processes (Kuang and Bretherton, 2006; Oueslati and Bellon, 2013; Sherwood *et al.*, 2013), if anything the results of the simulations suggest the opposite inference, namely a more modest climate sensitivity.

The present results are, at least in the broad sense, consistent with the findings of Zhao (2014) and Sherwood *et al.* (2014), which suggest that the representation of mixing processes explain a surprising amount of the intermodel spread in estimates of equilibrium climate sensitivity. They provide less support for the idea that the aspects of the mixing that are important for the climate sensitivity can be constrained by observations of the large-scale state, as for instance suggested by Fasullo and Trenberth (2012). Not only is the equilibrium climate sensitivity in the simulations analyzed here poorly correlated with the large-scale parameters, such as lower-tropospheric humidity or the strength of the overturning circulation, found to explain the intermodel spread in the multi-model ensemble analyzed by Fasullo and Trenberth (2012), different parameter combinations are shown to control the large-scale state as compared to the equilibrium climate sensitivity.

At most there is a relationship between the temperature of the base climate and the climate sensitivity of a model configuration, which results from the influence of convective parameters on clouds. Parameter choices that favour warmer climates also favour a greater reduction in the magnitude of short-wave cloud radiative effects with warming, and hence greater climate sensitivities. But exactly how this works remains unclear.

Of course certain connections identified in the present study, for instance the relation between the strength of the tropical circulation and the amount of total cloud cover may be different in an ensemble of structurally diverse climate models compared to the analyzed perturbed parameter ensemble – not because the physically based reasoning in the present study is flawed, but simply because there might be other differences among the models which we do not consider here.

Since key aspects of the simulations are sensitive to the most poorly represented processes, one should be cautious in physically over-interpreting the results. At best they point to the need to move beyond parameter studies, and purely statistical approaches, and to increasingly focus on improving our understanding and the representation of mixing processes in large-scale models. Here radiative convective equilibrium studies, which offer the capability of bridging the gap between cloud-resolving models and parametrized convection climate models (e.g. as in Popke *et al.*, 2013; Singh and O'Gorman, 2013), suggest a promising way forward.

Acknowledgements

We thank Florent Brient, Kerry Emanuel, Cathy Hohenegger, Thorsten Mauritsen, and Adam Sobel for helpful discussions, and Steven Sherwood, Sandrine Bony and Jean-Louis Dufresne, for sharing an early version of their manuscript. Support by Erich Roeckner in identifying key uncertain parameters of the climate model is gratefully acknowledged, as well as constructive comments on the manuscript by two anonymous reviewers. The research leading to these results has received funding from the European Union, Seventh Framework Programme (FP7/2007–2013) under grant agreement 244067

to the EUCLIPSE Project. AV was supported by the German Science Foundation under grant agreement VO 1765/3-1.

References

Betts AK. 1973. Non-precipitating cumulus convection and its parametrization. *Q. J. R. Meteorol. Soc.* **99**: 178–196, doi: 10.1002/qj.49709941915.

Bony S, Dufresne JL. 2005. Marine boundary-layer clouds at the heart of cloud feedback uncertainties in climate models. *Geophys. Res. Lett.* **32**: L20806, doi: 10.1029/2005GL023851.

Bony S, Dufresne JL, Treut HL, Morcrette J-J, Senior CA. 2004. On dynamic and thermodynamic components of cloud changes. *Clim. Dyn.* **22**: 71–86, doi: 10.1007/s00382-003-0369-6.

Bratley P, Fox BL. 1988. Algorithm 659: Implementing Sobol's quasi-random sequence generator. *ACM Trans. Math. Software* **14**: 88–100.

Brient F, Bony S. 2012. Interpretation of the positive low-cloud feedback predicted by a climate model under global warming. *Clim. Dyn.* **40**: 2415–2431, doi: 10.1007/s00382-011-1279-7.

Collins M, Booth B, Bhaskaran B, Harris G, Murphy J, Sexton D, Webb M. 2010. Climate model errors, feedbacks and forcings: A comparison of perturbed physics and multi-model ensembles. *Clim. Dyn.* **36**: 1737–1766.

Emanuel KA. 1995. On thermally direct circulations in moist atmospheres. *J. Atmos. Sci.* **52**: 1529–1534.

Emanuel KA, Neelin JD, Bretherton CS. 1994. On large-scale circulations in convecting atmospheres. *Q. J. R. Meteorol. Soc.* **120**: 1111–1143.

Fasullo JT, Trenberth KE. 2012. A less cloudy future: The role of subtropical subsidence in climate sensitivity. *Science* **338**: 792–794.

Frierson DMW. 2007. The dynamics of idealized convection schemes and their effect on the zonally averaged tropical circulation. *J. Atmos. Sci.* **64**: 1959–1976.

Gent PR, Willebrand J, McDougall T, McWilliams JC. 1995. Parameterizing eddy-induced tracer transports in ocean circulation models. *J. Phys. Oceanogr.* **25**: 463–474.

Giorgetta MA, Jungclaus JH, Reick CH, Legutke S, Brovkin V, Crueger T, Esch M, Fieg K, Glushak K, Gayler V, Haak H, Hollweg H-D, Ilyina T, Kinne S, Kornblueh L, Matei D, Mauritsen T, Mikolajewicz U, Mueller WA, Notz D, Raddatz T, Rast S, Redler R, Roeckner E, Schmidt H, Schnur R, Segschneider J, Six K, Stockhause M, Wegner J, Widmann H, Wieners K-H, Claussen M, Marotzke J, Stevens B. 2013. Climate and carbon cycle changes from 1850 to 2100 in MPI-ESM simulations for the coupled model intercomparison project phase 5. *J. Adv. Model. Earth Syst.* **5**: 572–597, doi: 10.1002/jame.20038.

Gregory JM, Ingram WJ, Palmer MA, Jones GS, Stott PA, Thorpe RB, Lowe JA, Johns TC, Williams KD. 2004. A new method for diagnosing radiative forcing and climate sensitivity. *Geophys. Res. Lett.* **31**: L03205, doi: 10.1029/2003GL018747.

Hartmann DL, Short DA. 1980. On the use of Earth radiation budget statistics for studies of clouds and climate. *J. Atmos. Sci.* **37**: 1233–1250.

Heinemann M, Jungclaus JH, Marotzke J. 2009. Warm Paleocene/Eocene climate as simulated in ECHAM5/MPI-OM. *Clim. Past* **5**: 785–802.

Held IM, Hou AY. 1980. Nonlinear axially symmetric circulations in a nearly inviscid atmosphere. *J. Atmos. Sci.* **37**: 515–533.

Joshi MM, Webb MJ, Maycock AC, Collins M. 2010. Stratospheric water vapor and high climate sensitivity in a version of the HadSM3 climate model. *Atmos. Chem. Phys.* **10**: 7161–7167.

Jungclaus J, Fischer N, Haak H, Lohmann K, Marotzke J, Matei D, Mikolajewicz U, Notz D, von Storch JS. 2013. Characteristics of the ocean simulations in the MPI earth system model. *J. Adv. Model. Earth Syst.* **5**: 422–446, doi: 10.1002/jame.20023.

Kuang Z, Bretherton CS. 2006. A mass-flux scheme view on a high-resolution simulation of a transition from shallow to deep cumulus convection. *J. Atmos. Sci.* **63**: 1895–1909.

Lott F. 1999. Alleviation of stationary biases in a GCM through a mountain drag parameterization scheme and a simple representation of mountain lift forces. *Mon. Weather Rev.* **127**: 788–801.

Mauritsen T, Stevens B, Röckner E, Crueger T, Esch M, Giorgetta M, Haak H, Jungclaus J, Klocke D, Matei D, Mikolajewicz U, Notz D, Pincus R, Schmidt H, Tomassini L. 2012. Tuning the climate of a global model. *J. Adv. Model. Earth Syst.* **4**: M00A01, doi: 10.1029/2012MS000154.

Medeiros B, Stevens B, Held IM, Zhao M, Williamson DL, Olson JG, Bretherton CS. 2008. Aquaplanets, climate sensitivity, and low clouds. *J. Clim.* **21**: 4974–4991.

Meraner K, Mauritsen T, Voigt A. 2013. Robust increase in equilibrium climate sensitivity under global warming. *Geophys. Res. Lett.* **40**: 5944–5948, doi: 10.1002/2013GL058118.

Möbis B, Stevens B. 2012. Factors controlling the position of the Intertropical Convergence Zone on an aquaplanet. *J. Adv. Model. Earth Syst.* **4**: M00A04, doi: 10.1029/2012MS000199.

Neelin JD, Held IM. 1987. Modeling tropical convergence based on the moist static energy budget. *Mon. Weather Rev.* **115**: 3–12.

Neggers RAJ, Neelin JD, Stevens B. 2007. Impact mechanisms of shallow cumulus convection on tropical climate dynamics. *J. Clim.* **20**: 2623–2642.

Nordeng T. 1994. *Extended Versions of the Convective Parametrization Scheme at ECMWF and their Impact on the Mean Transient Activity of the Model in the Tropics*, *Technical Memorandum* 206. ECMWF: Reading, UK.

Oueslati B, Bellon G. 2013. Convective entrainment and large-scale organization of tropical precipitation: Sensitivity of the CNRM-CM5 hierarchy of models. *J. Clim.* **26**: 2931–2946.

Pacanowski RC, Philander SGH. 1981. Parameterization of vertical mixing in numerical models of tropical oceans. *J. Phys. Oceanogr.* **11**: 1443–1451.

Popke D, Voigt A, Stevens B. 2013. Climate and climate change in a radiative convective equilibrium version of ECHAM6. *J. Adv. Model. Earth Syst.* **5**: 1–14.

Rieck M, Nuijens L, Stevens B. 2012. Marine boundary-layer cloud feedbacks in a constant relative humidity atmosphere. *J. Atmos. Sci.* **69**: 2538–2550.

Schneider T. 2006. The general circulation of the atmosphere. *Annu. Rev. Earth Planet. Sci.* **34**: 655–688.

Schneider T, Walker CC. 2008. Scaling laws and regime transitions of macroturbulence in dry atmospheres. *J. Atmos. Sci.* **65**: 2153–2173.

Schneider T, O'Gorman PA, Levine X. 2010. Water vapor and the dynamics of climate changes. *Rev. Geophys.* **48**: 1–23.

Sherwood SC, Hernandez-Deckers D, Colin M, Robinson F. 2013. Slippery thermals and the cumulus entrainment paradox. *J. Atmos. Sci.* **70**: 2426–2442.

Sherwood SC, Bony S, Dufresne JL. 2014. Spread in model climate sensitivity traced to atmospheric convective mixing. *Nature* **505**: 37–43.

Singh MS, O'Gorman PA. 2013. Influence of entrainment on the thermal stratification in simulations of radiative-convective equilibrium. *Geophys. Res. Lett.* **40**: 4398–4403, doi: 10.1002/grl.50796.

Sobel AH, Bretherton CS. 2000. Modeling tropical precipitation in a single column. *J. Clim.* **13**: 4378–4392.

Stevens B. 2006. Bulk boundary-layer concepts for simplified models of tropical dynamics. *Theor. Comput. Fluid Dyn.* **20**: 279–304.

Stevens B. 2007. On the growth of layers of non-precipitating cumulus convection. *J. Atmos. Sci.* **64**: 2916–2931.

Stevens B, Bony S. 2013a. Water in the atmosphere. *Phys. Today* **66**: 29–34.

Stevens B, Bony S. 2013b. What are climate models missing? *Science* **340**: 1053–1054.

Stevens B, Giorgetta M, Esch M, Mauritsen T, Crueger T, Rast S, Salzmann M, Schmidt H, Bader J, Block K, Brokopf R, Fast I, Kinne S, Kornblueh L, Lohmann U, Pincus R, Reichler T, Röckner E. 2013. Atmospheric component of the MPI earth system model: ECHAM6. *J. Adv. Model. Earth Syst.* **5**: 1–27, doi: 10.1002/jame.20015.

Taylor KE, Stouffer RJ, Meehl GA. 2012. An overview of CMIP5 and the experiment design. *Bull. Am. Meteorol. Soc.* **93**: 485–498.

Tiedtke M. 1989. A comprehensive mass flux scheme for cumulus parameterization in large-scale models. *Mon. Weather Rev.* **117**: 1779–1800.

Vecchi GA, Soden BJ. 2007. Global warming and the weakening of the tropical circulation. *J. Clim.* **20**: 4316–4340.

Vial J, Dufresne JL, Bony S. 2013. On the interpretation of inter-model spread in CMIP5 climate sensitivity estimates. *Clim. Dyn.* **41**: 3339–3362, doi: 10.1007/s00382-013-1725-9.

Voigt A, Abbot DS, Pierrehumbert RT, Marotzke J. 2011. Initiation of a Marinoan Snowball Earth in a state-of-the-art atmosphere–ocean general circulation model. *Clim. Past* **7**: 249–263.

Webb MJ, Senior CA, Sexton DMH, Ingram WJ, Williams KD, Ringer MA, McAvaney BJ, Colman R, Soden BJ, Gudgel R, Knutson T, Emori S, Ogura T, Tsushima Y, Andronova N, Li B, Musat I, Bony S, Taylor KE. 2006. On the contribution of local feedback mechanisms to the range of climate sensitivity in two GCM ensembles. *Clim. Dyn.* **27**: 17–38, doi: 10.1007/s00382-006-0111-2.

Zhao M. 2014. An investigation of the connections among convection, clouds and climate sensitivity in a global climate model. *J. Clim.* **27**: 1845–1862, doi: 10.1175/JCLI-D-13-00145.1.

